Materials Research Proceedings 41 (2024) 146-155 https://doi.org/10.21741/9781644903131-16

Comparison between ALE and Lagrangian finite element formulations to simulate tensile loading for FDM parts

HOMRANI Mohamed Khalil[1,a]*, DEMARBAIX Anthonin[2], RIVIERE-LORPHÈVRE Edouard[1], BEUSCART Thomas[1], OCHANA Imi[1,2], DUCOBU François[1]

[1]Machine Design and Production Engineering Lab – Research Institute for Science and material Engineering – University of Mons, Place du Parc 20, Mons, Belgium

[2]Science and Technology Research Unit – Science and Technology Department, HEPH-Condorcet University Square Hiernaux 2, 6000 Charleroi, Belgium

[a]Mohamedkhalil.homrani@umons.ac.be

Keywords: Finite Element, Tensile Testing, Arbitrary Lagrangian Eulerian, 3D Printing

Abstract. Material Extrusion (MEX) and by extension Fused Deposition Modeling (FDM) is a popular Additive Manufacturing (AM) process used to fabricate complex parts. FDM as of recent is no longer solely utilized for prototyping parts but also used for producing functional components in industrial and research applications. The investigation of material properties of these FDM parts by experimental means is a time-consuming task. Therefore, the use of numerical simulation methods is highly required. Since 1993, various Finite Element Analysis (FEA) models are found in literature attempting to effectively simulate FDM parts utilizing many formulations, each with their pros and cons. The present study aims to compare Lagrangian and Arbitrary Lagrangian-Eulerian (ALE) finite element formulations in simulating tensile loading for FDM parts. The efficiency and precision of the aforementioned methods is evaluated in the numerical simulation of the tensile loading of an ASTM D638 standard geometry ABS specimen utilizing both ABAQUS/Explicit and ABAQUS/Standard. Utilizing a paper from the literature for experimental validation, this study additionally provides insight into explicit and implicit models' computational efficiency, focusing on the advantages of explicit models for this application. The effects of mesh element type and size on results are also studied for each method. Based on these results, some useful guidelines for selecting the most suitable model of tensile loaded FDM parts are presented.

Introduction

The progress of Additive Manufacturing (AM) within the last few decades has been remarkable, with consistent double-digit growth, AM has transformed into a market valued at over $4 billion in 2015 [1]. Projections indicate that the AM market is expected to surpass $35.6 billion by 2024 [2]. This market expansion is primarily due to advances made through research, ranging from new findings in AM materials to studies with the goal of reducing costs by easing the development cycle [3]. This reduction can also be a consequence of the easing in research costs, increasingly digital alternatives such as digital twins and Finite Element Analysis (FEA) models allow for progress to be made at significantly reduced cost and time invested [4].

Within this manufacturing technology classification is Material Extrusion (MEX) [5], this category encompasses AM processes where material is selectively dispensed through a nozzle or orifice to print parts layer by layer. Fused Deposition Modeling (FDM) in particular starts with materials undergoing a liquefaction process. Subsequently, the liquefied material is precisely deposited layer by layer through a known diameter nozzle [6], aligning with the input Computer Assisted Drawing (CAD) model provided in .STL format [7]. The material gradually cools and solidifies layer by layer [8]. To allow solidification to occur, the heated bed temperature is

maintained lower than the extrusion temperature [9]. Afterward, post-processing techniques and geometry modifications are utilized to achieve the desired final shape [10].

An often-studied mechanical property that has the most reoccurring research in AM is tensile strength. This refers to the maximum amount of tensile stress a material can withstand before failure. Understanding the factors that influence it is essential to improve the printing process and achieve the desired part properties. Studies focusing on this property mainly utilize ASTM D638 types I to IV geometry [11]. This document is a standard test method published by the American Society for Testing and Materials (ASTM) that is used to determine the tensile properties of plastic materials. The anisotropy resulting from AM parts results in a significant discrepancy between the mechanical properties along different axes, this poses a unique challenge in testing mechanical strength across the construction direction of the printed parts.

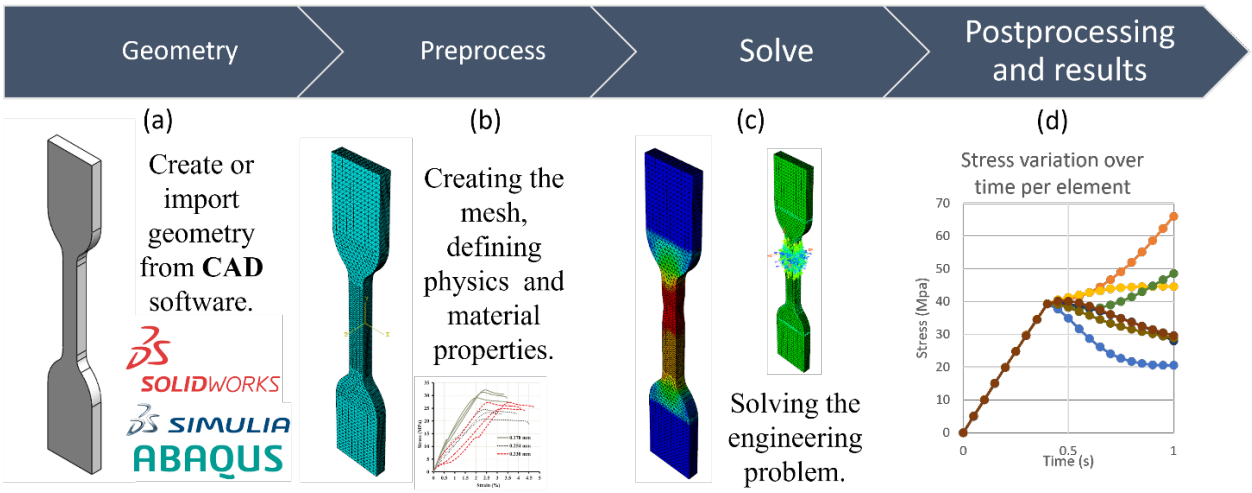

Figure 1: Typical finite element analysis steps, showing geometry creation (a), defining the mesh and material properties (b), solving (c), and results processing (d)

FEA has become an important and useful tool for solving complex eigenvalue problems, initial value, and boundary value problems. The workflow of which shown in Fig. 1 shows its simplicity which comes from representing each finite element as simple mesh geometry [12] which can be seen in Fig. 1.b. Furthermore, several recent optimizations have increased the popularity of FEA in research with the benefit of reducing development costs. As an example, we can take the study this work utilizes for experimental validation. Garg et al. [13] focus on the deformation of FDM samples, examining important printing parameters such as layer thicknesses and raster orientations under tension. FEA is conducted to simulate the elastoplastic behavior of ABS-printed specimens, the results of which are compared to experiments.

FE models can be performed implicitly or explicitly, with distinct differences and advantages to each. Explicit FE analysis is characterized by incrementally advancing the kinematic state from the previous increment; results from these models may deviate from experimental values if the time increment remains insufficiently low. These models often present stability problems: the results are only conditionally stable but still often offer significantly faster converging times with lower computational costs. Implicit analysis, on the other hand, iterates to determine the solution to a non-linear problem. It often provides better results for elastoplastic models while requiring significantly larger computational resources.

The two primary types of models encountered in the literature utilize Lagrangian, Eulerian, and Arbitrary Lagrangian-Eulerian (ALE) formulations, all popular candidates for FEA mathematical formulations [14]. The Eulerian formulation is used for large deformation problems. These problems are defined in a way where the mesh is fixed while the material moves freely through

the mesh. Despite being best suited for large deformation problems, Eulerian simulations are expensive in view of the computation time due to the advection step. Meanwhile, Lagrangian algorithms are used to assess material behavior under static, quasi-static, and dynamic loads, which induces deformations on the mesh. Each individual node in this mesh formulation is attached to the model. Advanced material simulations can still be implemented by this method. There are literature cases of Lagrangian method application in problems with large deformations, such as Thije et al. [17]. However, Lagrangian formulation is generally ill-suited for these problems since it usually terminates at an early stage of an extreme mesh distortion.

To bypass the issues plaguing the two prior mentioned methods, the ALE method is employed, which describes a broad range of analysis approaches, from purely Lagrangian analysis to purely Eulerian analysis. Typically, an ALE analysis follows an approach between these extremes. The ALE "Operator split" during each increment consists of a Lagrangian step where the mesh adheres to the material, an equilibrated "Lagrangian configuration" is computed at the next time increment, followed by an Eulerian step where a new mesh is defined. Finally, an advection step is performed where data is transferred from the old mesh to the new one.

The ALE formulation has been extensively used to model material cutting [15], with no prior applications in AM FEA studies. The goal of this study is to draw a direct comparison between the prior mentioned FE formulations in implicit and explicit simulations.

Development of the FE model

The simulation of the entire tensile test is recreated using ABAQUS/Standard and ABAQUS/Explicit for the finite element codes. In total, eight FE models were developed. Using Both Lagrangian and ALE techniques, each in explicit and implicit. All the created models consisting of a deformable dog-bone specimen in accordance with ASTM D638. The specimen geometry and dimensions are presented in Fig. 2(c), while gripper arrangement and loads are shown respectively in fig. 2(b) and 2(a).

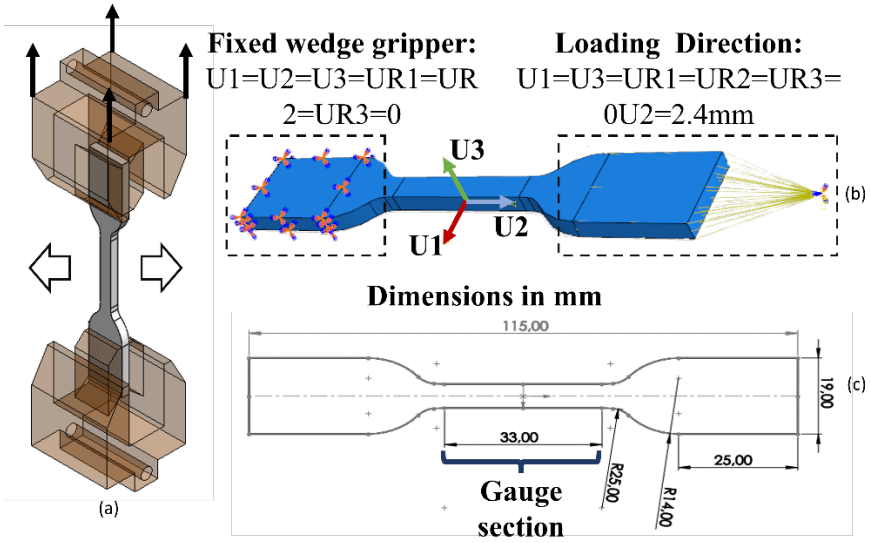

Figure 2: Boundary conditions applied to the model (a), experimental gripper arrangement (b), and ASTM D638 sample geometry (c)

The same loading conditions, summarized in Fig. 3(b), were used in the Lagrangian implicit, Lagrangian explicit, ALE implicit, and ALE explicit models to allow the comparison of the results. Similar to the tensile testing performed by the experimental validation paper Garg et al. [13], one end of the specimen is held in place while the displacement is applied from the other end, as schematically represented in Fig. 2(a). The boundary conditions applied are further demonstrated in Fig. 2(b) where an encastre constraint is placed on one end of the dog bone by limiting all six

degree of freedoms, U1=U2=U3=UR1=UR2=UR3=0. The displacement along axis is then applied from the other end as U1=U3=UR1=UR2=UR3=0, U2= displacement at failure= 2.4 mm (taken from experimental validation study [13]). Simulation time is fixed to one second for all models to match the experimental load time also equal to 1 second. The material properties applied in the following FE models are also shown in Fig. 3(a) and 3(c) as seen in Anton et al. [16]. Implementing these properties was done identically to the experimental validation paper Garg et al. [13]. First, by converting the engineering stress/strain curve into true stress/strain using the ABAQUS material calibration tool. The resulting true stress/strain curve is then used to create an elastic plastic isotropic material within the same ABAQUS material calibration tool. The material model is interpolated to the elastic modulus in Fig. 3(c), which is calculated from the selected yield point shown in Fig. 3(a) at 35.928 MPa (with a corresponding strain of 0.01633 mm/mm).

The Von Mises Yield Criterion is used to model the material with isotropic hardening using the calculated plastic deformation part of the true stress/strain data obtained from the previous step.

The FDM samples created in CAD software SolidWorks are imported to ABAQUS for the FE simulation under the unidirectional tensile loading, with the goal of studying their elastic-plastic deformation. The analysis is initially carried out utilizing the Lagrangian formulation in implicit and explicit schemes, and the modeling is considered as a load/displacement problem.

(a)

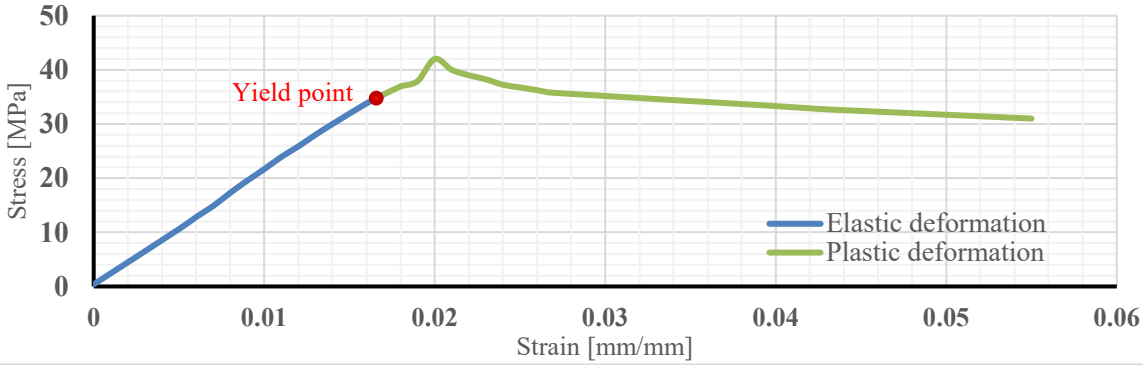

(b)

Simulation time	1 s
Displacement	2.4 mm

(c)

Density	1.04 g/cm^3
Elastic modulus	2200 MPa
Poisson ratio	0.35

Figure 3: Stress/strain curve of the ABS material from Anton et al. [16] (a), loading conditions (b), and ABS material properties (c)

As previously discussed, one of the requirements to run a FE simulation is to fragment the simulated part into mesh cells. By performing a mesh sensitivity study, it becomes possible to understand how different mesh configurations affect the model's results, this helps identify which meshes produce accurate results while minimizing redundant computational costs. The results of this analysis are shown in Fig. 4, the mesh element kept identical to the validation study [13] which is C3D4 (Continuum 3-dimensional 4-noded solid linear tetrahedron). Finer mesh size improves accuracy but demands higher computational resources, thus the model is meshed by tetrahedron elements. For consistency purposes, both implicit and explicit Lagrangian simulations are meshed with 1 mm elements while reducing the gauge element size to 0.5 mm (section shown in Fig. 2(c)).

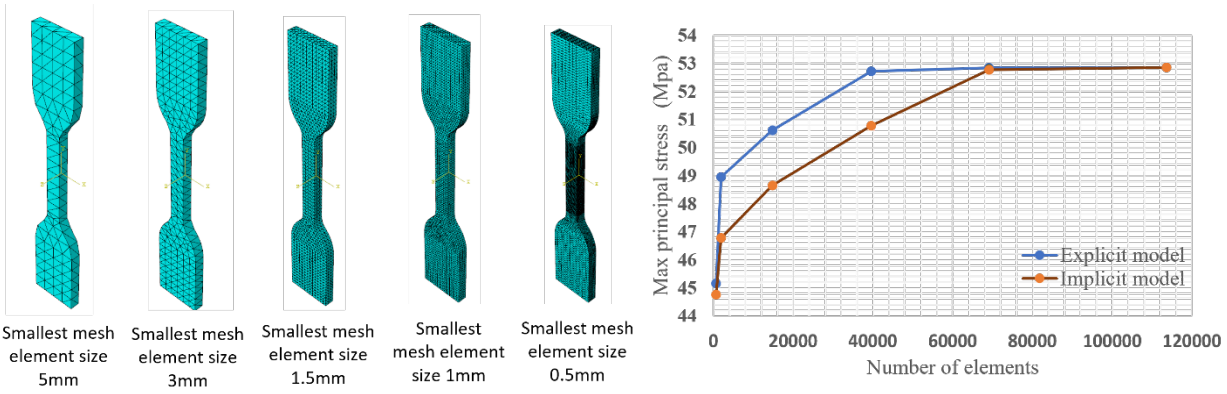

Figure 4: Simulation mesh sensitivity study

Lagrangian formulation

The first step of this study consists of replicating the findings of the experimental validation study by Garg et al. [13], this was achieved by replicating the available simulation parameters. The FE simulations are conducted with ABAQUS/Standard, then with ABAQUS/Explicit for the same material model created with the same material parameters as the reference paper [13]. The output database results of the two simulations are then extracted by selecting multiple nodes in the necking region and comparing results to the validation paper. Simulated results are subsequently validated and compared with the experimental observations from Garg et al. [13].

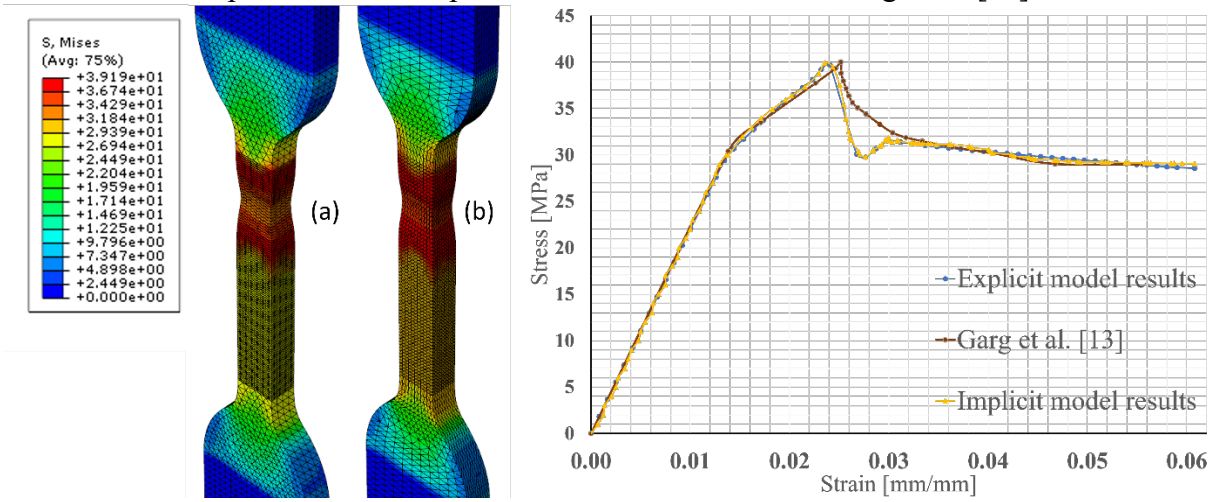

Figure 5: Deformed mesh results comparison between implicit (a), explicit simulation (b) both showing Von Mises equivalent stress and resulting stress/strain compared with Garg et al. [13].

Initial mesh deformation analysis shown in Fig. 5 demonstrates good agreement between the implicit, explicit, and validation paper results.

The initial results show good agreement between implicit and explicit simulation results with the experimental validation paper while the material is exhibiting elastic properties, then briefly diverges as material behavior transitions into plastic deformation before converging again for the rest of the curve. This discrepancy between the results could be due to the input properties of the models being slightly different, as the ABS material parameters were obtained utilizing Optical Character Recognition (OCR) software and not a numerical database. The difference could also be due to any of the missing study parameters in the reference [13] such as mesh parameters, deformation rate or loading parameters.

For explicit solvers, the computational cost of a single increment is expectedly low. However, it is necessary to maintain a low time increment since the solution could become unstable as error margins increase rapidly. The largest viable time increment is calculated by ABAQUS/explicit

when mass scaling is not in use, is called a stable time increment (STI). On the other hand, the computational cost of implicit increments is significantly larger, If the system proves to be nonlinear, the solution needs to be calculated multiple times per increment. Thus, the more nonlinear a problem is, the more computationally expensive it is to converge on a valid solution.

A comparison of computation time is established in Table 1, showing an efficiency discrepancy between the implicit and explicit solver for this type of problem. Even when no mass scaling is in use to reduce computation time, explicit models prove to be more computationally efficient. An Intel Core i7-12650H was used for all simulations, with the advent of GPU acceleration being only available for the implicit solver where a GeForce RTX 3070M aids in reducing computation time.

Table 1: Computation time comparison between the implicit and explicit solvers

Solver type	Parallelization	Mesh element type	computation time	Max principal stress (MPa)
Implicit	8-core CPU	C3D4	27 hrs 44 min 32 sec	39.19
Implicit	CUDA GPU	C3D4	8 hrs 27 min 38 sec	39.19
Implicit	8-core CPU/GPU	C3D4	6 hrs 9 min 15 sec	39.19
Implicit	8-core CPU/GPU	C3D8	5 hrs 32 min 34 sec	39.19
Explicit	8-core CPU	C3D4	7 hrs 17 min 31 sec	39.72
Explicit	8-core CPU	C3D8	4 hrs 5 min 7 sec	39.72

As prior mentioned, further reduction in computational costs can be achieved by utilizing mass scaling, which increases the material density while keeping resulting calculations unaffected. A study was conducted with the goal of further reducing computational time by testing various STIs, the resulting plastic deformation section (see Fig. 3(a)) of the stress strain curves obtained from each simulation are shown in Fig. 6 since results perfectly coincided during elastic deformation. Results of computation time are shown in Table 2.

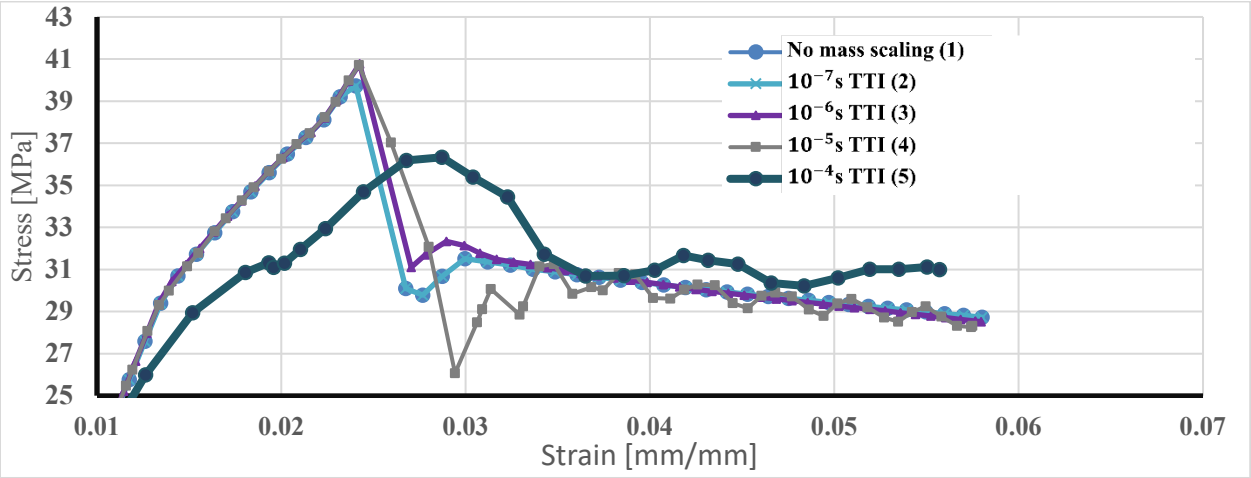

Figure 6: Mass scaling sensitivity study

When no mass scaling is in use, the STI calculated by ABAQUS/explicit hovers around 10^{-7}s. This value explains why defining a target time increment (TTI) of a similar magnitude creates perfectly coinciding graphs, as can be seen in Fig. 6. Once the defined TTI value differs greatly from the default STI value, deviations in the resulting stress strain curve occur. A simple explanation to this increasing deviation is that as we increase the TTI, ABAQUS begins to modify the density of more and more mesh elements which now have a smaller STI, resulting in a material

model that contradicts the physical nature of the material. Another issue that could arise from increasing the TTI is unstable solutions, which induces spurious variations in the resulting properties of the model, an example of this is seen in the stress strain curve (4) in Fig. 6 where the stress value oscillates sporadically around the stable value of no mass scaling.

Table 2 summarizes the time of analysis at the which utilized 8 cores of the processor Intel i7-12650H for all simulations. It can be observed that the increase in target time increment results in an increase of the percent of mass increased (m%).

Table 2: Resulting processing time of each mass scaling simulation

Target time increment (s)	CPU time	m (%)
1e-7	7 hrs 2 min 31 sec	0.121
1e-6	4 hrs 33 min 16 sec	2.874
1e-5	0 hrs 3 min 38 sec	10.183
1e-4	0 hrs 0 min 31 sec	23.784
1e-3	0 hrs 0 min 15 sec	38.742

Due to the addition of non-physical mass that has a proven impact on the accuracy of our study, the energy balance is to be studied. The kinetic energy should not exceed 5% of internal energy [18]. Fig. 7 demonstrates two examples of performed simulations, the first highlighting the energy output of the TTI=1e-6s which passes the 5% kinetic energy/Internal energy ratio rule, while the second of TTI=1e-4s fails to meet the criteria.

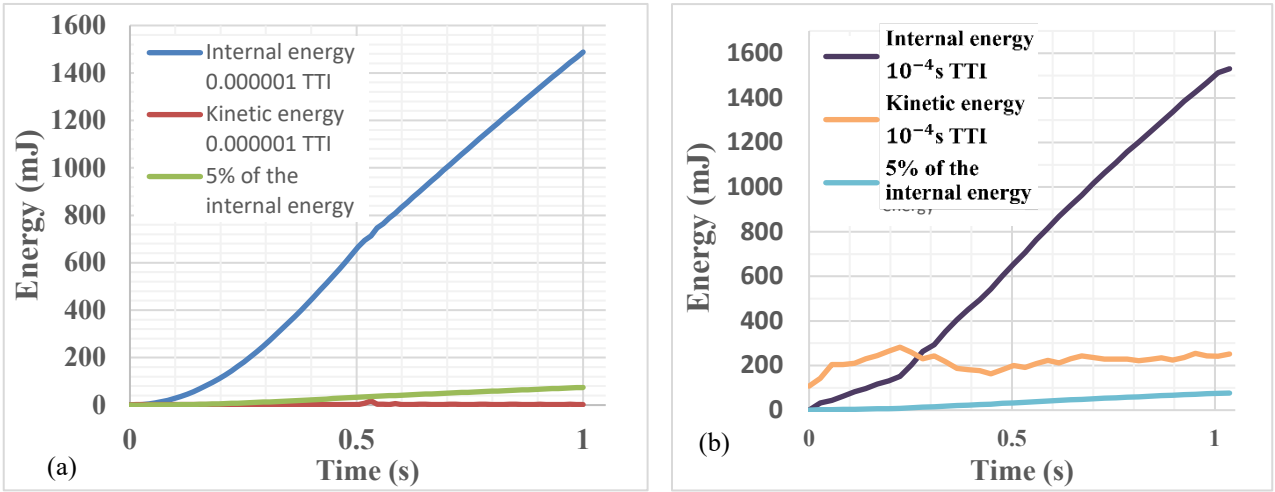

Figure 7: Differences of internal energy and kinetic energy at TTI=1e-6 (a) and TTI=1e-4 (b)

Arbitrary Lagrangian Eulerian formulation

Similar to the previous section, two FE simulations are conducted with ABAQUS/Standard then the same is done with ABAQUS/Explicit for the same material model created with the same material parameters as the paper. The output database results are then extracted from the necking region and compared to previous results utilizing the Lagrangian formulation. The simulated results are subsequently validated and compared with the experimental observations from Garg et al. [13] as previously done.

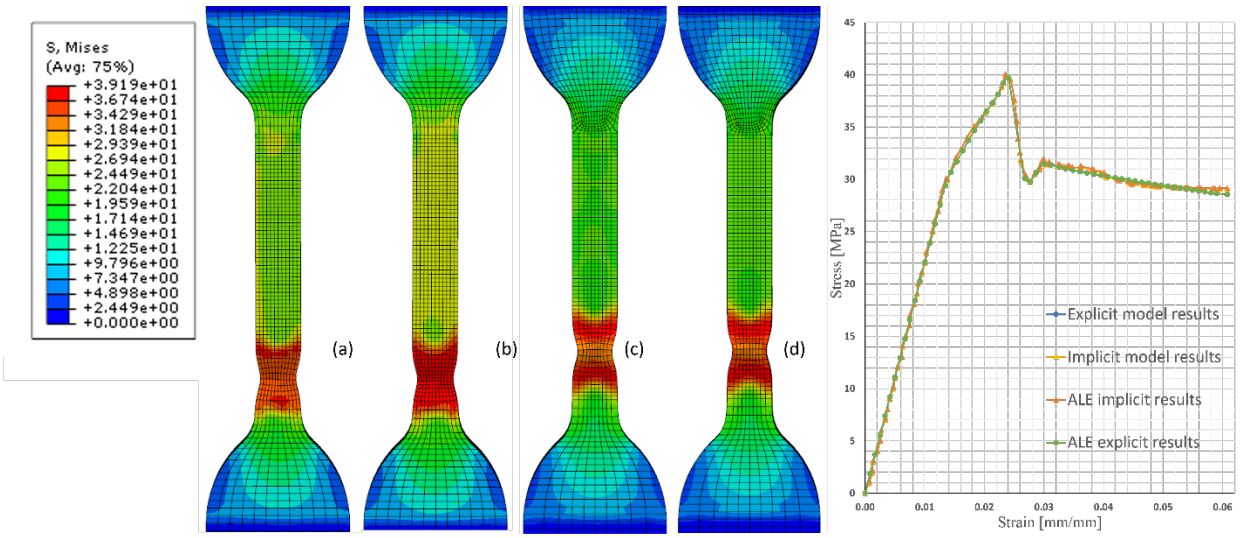

Figure 8: Deformed mesh results comparison between Lagrangian explicit simulation (a), ALE explicit simulation (b), Lagrangian implicit simulation (c), and ALE implicit simulation (d) all showing Von Mises equivalent stress distribution and resulting stress/strain curve.

Analysis shown in Fig. 8 demonstrates good agreement between the implicit, explicit, and validation paper results. The mesh element type utilized for results comparison Lagrangian explicit and ALE explicit was modified to C3D8 (8-node linear brick) to match the Lagrangian implicit and ALE implicit mesh type, this was done due to the ABAQUS solver limitations which only allows ALE formulations on a limited selection of element types within ABAQUS/standard. A mesh sensitivity study was performed for this element type and an appropriate mesh size was selected in accordance with it (1 mm element size with 0.5 mm elements for the gauge section).

A similar comparison of computation time is established in Table 3, showing an expected efficiency discrepancy between the Lagrangian and ALE algorithms for both implicit and explicit solutions.

Table 3: Computation time comparison between the implicit Lagrangian and implicit ALE then between explicit Lagrangian and explicit ALE (Explicit Lagrangian taken as reference study)

Solver type	Formulation	Mass scaling	Parallelization	computation time (s)	Max principal stress (MPa)
Implicit	Lagrangian		8-core CPU/GPU	+32.00% time	39.19
Implicit	ALE		8-core CPU/GPU	+228.18% time	38.41
Explicit	Lagrangian	None	8-core CPU	4 hrs 5 min 7 sec	39.72
Explicit	Lagrangian	1e-6s TTI	8-core CPU	-46.11% time	39.53
Explicit	ALE	None	8-core CPU	+68.23% time	38.74
Explicit	ALE	1e-6s TTI	8-core CPU	+7.09% time	38.68

The ALE formulation fails to provide a clear advantage in comparison with the Lagrangian models, after rigorous testing. Rather than demonstrating a positive outcome, ALE models raised concerns about computational efficiency without positive outcomes to match. Problems encountered with convergence time make the ALE formulation ineffective, thus questioning its application validity in this type of problem. The shortcomings of the ALE formulation in terms of convergence time compared to the Lagrangian method can be explained by the added advection step. The lack of a significant difference in results on the other hand can be explained by the low

deformation that the mesh exhibits, which makes utilizing the ALE formulation that is most effective with high deformation problems counterproductive.

Conclusions

Within this study, a series of comparisons were performed between the results and performance of implicit and explicit solvers utilized for analyzing AM ASTM D638 samples under uniaxial tensile loading. Such comparison should be of high interest to researchers modeling FE studies of AM parts, as it provides a guideline to selecting an optimal solver while verifying correct results using these different solving algorithms. Initial results highlight that stress-strain results from both solvers are near identical. This proves that either of the solvers can be effectively utilized, depending on simulation parameters. The explicit solver performed faster than the implicit solver on the same hardware, but the implicit solver presents the option to utilize GPU acceleration, which significantly lessens the gap in computation time. When mass scaling and load-rate-increase assumptions were used, the gap in computational efficiency widens anew, with the explicit model performing significantly faster than implicit.

A standard energy balance study was performed to assess the validity of the simulations when utilizing mass scaling to reduce computation costs. Based on the series of explicit dynamic studies at various mass scaling values, the results of the energy balance study shows that target time increments TTI=1e−6s is an appropriate value to significantly reduce analysis time.

Finally, a series of simulations based on the ALE formulation were proposed to numerically simulate the deformation of the specimens. ALE and classical Lagrangian simulations had to be successfully carried out with a new mesh element type C3D8 due to ABAQUS/standard limitations that allows ALE formulations on a limited selection of element types. Although the considered ALE model does not present any result improvement with neither the implicit nor explicit solvers and cannot achieve a comparable CPU time savings to the Lagrangian one, this is due to the ALE formulation's usefulness in high deformation studies, which this particular problem of tensile loading does not generally possess.

Perspectives

While the ALE formulation does not present any clear advantages when it comes to FE simulations of tensile testing AM specimen during plastic deformation. Further investigation needs to be conducted on the benefits of carrying it on models continuing until material fracture, as the specimen often exhibit extreme deformations right before when fracture occurs. Utilizing the ALE formulation could help provide more accurate fracture behavior predictions for AM parts under uniaxial tensile loading.

Acknowledgements

The authors would like to thank Région Wallonne for supporting this research as part of the SKYWIN ICOM2C3D research project under grant 8820.

References

[1] Terry T Wohlers and Tim Caffrey. Wohlers report 2015: 3d printing and additive manufacturing state of the industry annual worldwide progress report. 2015.

[2] Babak Kianian. Wohlers report 2019: 3d printing and additive manufacturing state of the industry, annual worldwide progress report. 2019.

[3] Bhrigu Ahuja, Michael Karg, and Michael Schmidt. Additive manufacturing in production: challenges and opportunities. Laser 3d manufacturing II, 9353: 11–20. https://doi.org/10.1117/12.2082521

[4] Ben Terrell. Faster FEA improves productivity and saves tens of thousands of dollars. Read on https://resources.sw.siemens.com/en-US/case-study-aquila-engineering the 6th of December 2023.

[5] Vidya Kishore and Ahmed Arabi Hassen. Polymer and composites additive manufacturing: material extrusion processes. In Additive Manufacturing, pages 183–216. 2021. https://doi.org/10.1016/B978-0-12-818411-0.00021-5

[6] Chua Chee Kai. Three-dimensional rapid prototyping technologies and key development areas. Computing & Control Engineering Journal, 5(4):200–206, 1994. https://doi.org/10.1049/cce:19940407

[7] Nicholas A Conzelmann, Lovro Gorjan, Fateme Sarraf, Lily D Poulikakos, Manfred N Partl, Christoph R Müller, and Frank J Clemens. Manufacturing complex Al2O3 ceramic structures using consumer-grade fused deposition modelling printers. Rapid Prototyping Journal, 26(6):1035–1048. https://doi.org/10.1108/RPJ-05-2019-0133

[8] Kai CC. Three-dimensional rapid prototyping technologies and key development areas. Computing & Control Engineering Journal. 1994 Aug 1;5(4):200-6.

[9] MS Khan and JP Dash. Enhancing surface finish of fused deposition modelling parts. 3D printing and additive manufacturing technologies, pages 45–57, 2019. https://doi.org/10.1007/978-981-13-0305-0 5

[10] Ian Gibson. Additive manufacturing technologies 3d printing, rapid prototyping, and direct digital manufacturing. 2015. https://doi.org/10.1007/978-1-4939-2113-3 21

[11] ASTM D638-14, “Standard Test Method for Tensile Properties of Plastics”, American Society for Testing and Materials. https://doi.org/10.1520/D0638-14

[12] Xiaoqing Wang and Kevin Chou. Microstructure simulations of inconel 718 during selective laser melting using a phase field model. The International Journal of Advanced Manufacturing Technology, 100:2147–2162, 2019. https://doi.org/10.1007/s00170-018-2814-z

[13] Ashu Garg and Anirban Bhattacharya. An insight to the failure of fdm parts under tensile loading: finite element analysis and experimental study. International Journal of Mechanical Sciences, 120:225–236, 2017. https://doi.org/10.1016/j.ijmecsci.2016.11.032.

[14] Olivier Pantalé, J-L Bacaria, Olivier Dalverny, Roger Rakotomalala, and Serge Caperaa. 2d and 3d numerical models of metal cutting with damage effects. Computer methods in applied mechanics and engineering, 193(39-41):4383– 4399, 2004. https://doi.org/10.1016/j.cma.2003.12.062

[15] Pedro Jose Arrazola, Tugrul Ozel, Domenico Umbrello, M Davies, and Ibrahim S Jawahir. Recent advances in modelling of metal machining processes. Cirp Annals, 62(2):695–718, 2013. https://doi.org/10.1016/j.cirp.2013.05.006

[16] Schmailzl Anton, Amann Thomas, Glockner Markus, and Fadanelli Martin. Finite element analysis of thermoplastic probes under tensile load using ls- dyna compared to ansys wb 14 in correlation to experimental investigations. In Proceedings of the ANSYS conference & 30th CADFEM users’ meeting, 2012.

[17] RHW Ten Thije, and Remko Akkerman. Large deformation simulation of anisotropic material using an updated Lagrangian finite element method. Computer methods in applied mechanics and engineering, 196(33-34):3141–3150,2007. https://doi.org/10.1016/j.cma.2007.02.010

[18] Min W, He Y, Sun ZC, Guo LG, Ou XZ. Dynamic explicit FE modeling of hot ring rolling process. Transactions of Nonferrous Metals Society of China. 2006 Dec 1;16(6):1274-80.